Single-subject classification of presymptomatic frontotemporal dementia mutation carriers using multimodal MRI

Rogier A. Feis[a,b,*], Mark J.R.J. Bouts[a,b,c], Jessica L. Panman[a,d], Lize C. Jiskoot[a,d], Elise G.P. Dopper[a,d,e], Tijn M. Schouten[a,b,c], Frank de Vos[a,b,c], Jeroen van der Grond[a], John C. van Swieten[d,f], Serge A.R.B. Rombouts[a,b,c]

[a] Department of Radiology, Leiden University Medical Centre, Leiden, Netherlands
[b] Leiden Institute for Brain and Cognition, Leiden University, Leiden, Netherlands
[c] Institute of Psychology, Leiden University, Leiden, Netherlands
[d] Department of Neurology, Erasmus Medical Centre, Rotterdam, Netherlands
[e] Alzheimer Centre & Department of Neurology, Neuroscience Campus Amsterdam, VU University Medical Centre, Amsterdam, Netherlands
[f] Department of Clinical Genetics, Neuroscience Campus Amsterdam, VU University Medical Centre, Amsterdam, Netherlands

ARTICLE INFO

ABSTRACT

Background: Classification models based on magnetic resonance imaging (MRI) may aid early diagnosis of frontotemporal dementia (FTD) but have only been applied in established FTD cases. Detection of FTD patients in earlier disease stages, such as presymptomatic mutation carriers, may further advance early diagnosis and treatment. In this study, we aim to distinguish presymptomatic FTD mutation carriers from controls on an individual level using multimodal MRI-based classification.

Methods: Anatomical MRI, diffusion tensor imaging (DTI) and resting-state functional MRI data were collected in 55 presymptomatic FTD mutation carriers (8 microtubule-associated protein Tau, 35 progranulin, and 12 chromosome 9 open reading frame 72) and 48 familial controls. We calculated grey and white matter density features from anatomical MRI scans, diffusivity features from DTI, and functional connectivity features from resting-state functional MRI. These features were applied in a recently introduced multimodal behavioural variant FTD (bvFTD) classification model, and were subsequently used to train and test unimodal and multimodal carrier-control models. Classification performance was quantified using area under the receiver operator characteristic curves (AUC).

Results: The bvFTD model was not able to separate presymptomatic carriers from controls beyond chance level (AUC = 0.582, p = 0.078). In contrast, one unimodal and several multimodal carrier-control models performed significantly better than chance level. The unimodal model included the radial diffusivity feature and had an AUC of 0.642 (p = 0.032). The best multimodal model combined radial diffusivity and white matter density features (AUC = 0.684, p = 0.004).

Conclusions: FTD mutation carriers can be separated from controls with a modest AUC even before symptom-onset, using a newly created carrier-control classification model, while this was not possible using a recent bvFTD classification model. A multimodal MRI-based classification score may therefore be a useful biomarker to aid earlier FTD diagnosis. The exclusive selection of white matter features in the best performing model suggests that the earliest FTD-related pathological processes occur in white matter.

1. Introduction

Frontotemporal lobar degeneration is a common cause of early-onset dementia with a similar prevalence to Alzheimer's disease in the presenile population (Ratnavalli et al., 2002; Harvey et al., 2003; Rabinovici and Miller, 2010; Seelaar et al., 2011; Rascovsky et al., 2011). Although there are clinical disease criteria for the different clinical variants of frontotemporal dementia (FTD) (Rascovsky et al., 2011; Gorno-Tempini et al., 2011), diagnosis is often complicated and delayed by clinical heterogeneity. This hinders clinicians in providing accurate prognosis, effective disease management and developing new treatments (Mohs et al., 2001; Mendez et al., 2007; Mendez, 2009; Pressman and Miller, 2014).

Multimodal magnetic resonance imaging (MRI) has been suggested as a promising biomarker to improve on diagnostic standards in FTD. In FTD patients, MRI revealed specific patterns of neurodegeneration, involving grey matter (GM) and white matter (WM) atrophy (Whitwell and Jack, 2005; Whitwell et al., 2012; Möller et al., 2015a; Möller et al., 2015b; Whitwell et al., 2015; Chao et al., 2007; Rabinovici et al., 2008; Seeley et al., 2009; Frings et al., 2014; Zhang et al., 2011; Pan et al., 2012; Risacher and Saykin, 2013), differences in diffusion tensor imaging (DTI) measures (Möller et al., 2015b; Zhang et al., 2011; Zhang et al., 2009; Agosta et al., 2012; McMillan et al., 2012; McMillan et al., 2014; Mahoney et al., 2014; Daianu et al., 2016), and differences in functional connectivity (Zhou et al., 2010; Zhou and Seeley, 2014; Farb et al., 2013; Lee et al., 2014; Hafkemeijer et al., 2015; Hafkemeijer et al., 2016).

These patterns have subsequently been utilised on an individual level to create MRI-based classification algorithms that can discriminate between FTD patients and control subjects (McMillan et al., 2014; Davatzikos et al., 2008; Raamana et al., 2014; Koikkalainen et al., 2016; Wang et al., 2016; Meyer et al., 2017; Bron et al., 2017; Bouts et al., 2018). Accurate classification of FTD patients using MRI measures is an important step towards a more substantiated diagnostic standard. However, most classification models are based on established FTD cases, limiting generalisability in patients who are at an earlier disease stage. Still, detection of these early-stage FTD cases is necessary to facilitate precise subject recruitment into clinical trials and potential early treatment with disease-modifying drugs (Huey et al., 2008).

In order to characterise FTD pathophysiology at an earlier stage, presymptomatic carriers of autosomal dominant FTD gene mutations were compared to controls in MRI group analyses (Borroni et al., 2008; Whitwell et al., 2011; Cash et al., 2018; Borroni et al., 2012; Rohrer et al., 2013; Premi et al., 2014; Dopper et al., 2014; Rohrer et al., 2015; Lee et al., 2017; Bertrand et al., 2018; Papma et al., 2017). Carriers of the three most common FTD gene mutations microtubule-associated protein Tau (*MAPT*), progranulin (*GRN*), and chromosome 9 open reading frame 72 (C9orf72) show brain alterations on MRI, even well before symptom onset. In these subjects, WM diffusivity changes (Borroni et al., 2008; Dopper et al., 2014; Papma et al., 2017) and functional connectivity changes (Whitwell et al., 2011; Borroni et al., 2012; Premi et al., 2014; Dopper et al., 2014) are often, but not exclusively (Lee et al., 2017; Bertrand et al., 2018; Papma et al., 2017), found in the absence of GM atrophy, suggesting that changes in the functional architecture and WM tracts may precede structural deterioration in the GM (Rohrer et al., 2013). Nonetheless, multi-centre analyses of a large international cohort show GM loss in *MAPT*, *GRN* and *C9orf72* carriers even before conversion (Cash et al., 2018; Rohrer et al., 2015). Although these presymptomatic group differences give insight into the pathophysiological mechanisms of FTD, individual heterogeneity complicates its utility in FTD diagnosis. Therefore, translation from group differences to single-subject classification models is imperative.

The present study brings two research areas together: we combine machine learning with presymptomatic FTD mutation carriers to study individual classification of FTD-pathology at an early stage. Our aim is to distinguish individual presymptomatic FTD mutation carriers from healthy controls using multimodal MRI.

2. Methods

2.1. Design

In order to distinguish presymptomatic FTD mutation carriers from controls, we applied two models. First, we applied a recent behavioural variant FTD (bvFTD)-control classification model (Bouts et al., 2018) to our MRI data to investigate whether the model separates presymptomatic mutation carriers from controls. We shall refer to this model as the "bvFTD model". In a second analysis, we trained a new classification model on the presymptomatic mutation carriers and controls' data, which we evaluated using cross-validation. We shall refer to this model as the "carrier-control model". MRI pre-processing, feature selection and classification were performed identically to previous work (Bouts et al., 2018).

2.2. Participants

This retrospective study partially included previously published (Dopper et al., 2014; Papma et al., 2017; Jiskoot et al., 2016) and newly acquired data from the Erasmus Medical Centre and Leiden University Medical Centre. Participants and clinical investigators were blinded to the participants' DNA status. The study was conducted in accordance with regional regulations and the Declaration of Helsinki. The Erasmus Medical Centre and Leiden University Medical Centre local medical ethics committees approved the study, and every participant provided written informed consent.

For the current study, we included 55 presymptomatic FTD mutation carriers (8 *MAPT*, 35 *GRN*, 12 *C9orf72*) and 48 healthy familial controls (6 *MAPT* family, 31 *GRN* family and 11 *C9orf72* family) between May 2010 and March 2016. These subjects were recruited from a cohort of healthy first-degree relatives of FTD patients with either a *MAPT*, *GRN* or *C9orf72* mutation (FTD-Risk Cohort; FTD-RisC) and visited the Erasmus Medical Centre for a one-day assessment in order to ascertain asymptomatic status, collect clinical data, and determine DNA status as described before (Dopper et al., 2014; Papma et al., 2017; Jiskoot et al., 2016). Participants were considered asymptomatic in the absence of (1) behavioural, cognitive, or neuropsychiatric change reported by the participant or knowledgeable informant, (2) cognitive disorders on neuropsychiatric tests, (3) motor neuron disease signs on neurologic examination, and (4) other FTD (Rascovsky et al., 2011; Gorno-Tempini et al., 2011) or amyotrophic lateral sclerosis (Ludolph et al., 2015) criteria. Healthy controls were assumed to have equal FTD risk as the general population. For a more detailed description of the recruitment protocol, see earlier work (Dopper et al., 2014; Papma et al., 2017; Jiskoot et al., 2016). Inclusion criteria for the current study were: age between 40 and 70 years, and availability of a T_1-weighted 3-dimensional MRI ($3DT_1$w) scan, a diffusion-weighted imaging (DWI) dataset, and a resting-state fMRI T_2*-weighted (rs-fMRI) scan. Exclusion criteria were: current or past neurologic or psychiatric disorders, history of drug abuse, large image artefacts, and gross brain pathology other than atrophy.

For details on the sample on which the bvFTD model was trained, please refer to Bouts et al. (2018) (Bouts et al., 2018). In short, 23 bvFTD patients and 35 controls between 40 and 80 years old were included to undergo a clinical assessment and MRI between November 2009 and November 2012. The MRI acquisition protocol was similar to the protocol applied in the current sample of carriers and controls. Image processing steps were identical to processing steps in the current sample.

2.3. MRI data acquisition

All subjects were scanned at the Leiden University Medical Centre using a 3 T MRI scanner (Achieva, Philips Medical Systems, Best, The Netherlands) with an 8-channel SENSE head coil. The imaging protocol included a whole-brain near-isotropic 3DT$_1$w sequence for cortical and subcortical tissue-type segmentation, a DWI sequence for assessments of white matter integrity, and a rs-fMRI for the calculation of functional connectivity measures. Participants were instructed to lie still with their eyes closed and not to fall asleep during rs-fMRI. For scan parameters, see Table 1.

2.4. Image pre-processing

For 3DT$_1$w images, the following pre-processing steps were performed: bias field correction (N4ITK (Tustison et al., 2010)), brain extraction (FSL BET (Smith, 2002)), non-linear registration to the MNI152 2 × 2 × 2 mm T1 template (FNIRT (Anderson et al., 2007)), tissue-type segmentation (SPM12 (Friston et al., 2007)) and segmentation of deep grey matter structures, including the bilateral thalamus, caudate nucleus, putamen, globus pallidus, nucleus accumbens, amygdala and hippocampus (FIRST (Patenaude et al., 2011)).

Pre-processing for DTI datasets included correction of motion and eddy-current induced distortion (eddy correct (Leemans and Jones, 2009)), calculation of voxel-wise measures of fractional anisotropy (FA), mean diffusivity (MD), axial diffusivity (AxD, largest eigenvalue), and radial diffusivity (RD, average of the two remaining eigenvalues, DTIFIT (Smith et al., 2004)). A global mean FA image was created by nonlinearly registering FA maps to the FMRIB58_FA template, and tract-based spatial statistics (FSL TBSS (Smith et al., 2006)) was used to extract FA, MD, AxD and RD values using the standard FSL TBSS skeleton. The skeleton was thresholded at 0.2 to ensure skeleton extracted values originate from WM.

For rs-fMRI data, pre-processing included motion correction (Jenkinson et al., 2002), brain extraction, spatial smoothing using a Gaussian kernel with a full width at half maximum of 3 mm, grand mean intensity normalisation, motion artefact removal, and high-pass temporal filtering (cut-off frequency = 0.01 Hz). Motion artefacts were removed using a single-session independent component analysis (ICA) to decompose the rs-fMRI data into distinct statistically independent components. Subsequently, motion-related components were automatically identified and removed using the ICA-based automatic removal of motion artefacts (ICA-AROMA, version 0.3-beta) procedure (Pruim et al., 2015). Registration to standard space was performed in two steps. First, a temporal mean image calculated from the 4D rs-fMRI volume was registered to the 3DT1w image using Boundary-Based Registration (Greve and Fischl, 2009). Next, resulting registration parameters were concatenated to the 3DT$_1$w-to-MNI152 template registration parameters to obtain the final registration parameters.

All registration and segmentation steps were critically reviewed and errors were corrected accordingly.

2.5. Feature selection

Cortical GM density (GMD) and WM density (WMD) were calculated as a weighted average of their respective regional WM or GM probability (SPM segmentation) weighted by the probability of a voxel being part of that specific tract or region. The latter probabilities were derived from the 48 Harvard-Oxford probabilistic anatomical brain atlas cortical regions (split into left and right) and from the Johns-Hopkins University white-matter tractography atlas for 20 WM tract regions. Voxels with region probability values < 25% were excluded. This provided a measure of brain atrophy of a specific GM region or WM tract. For deep GM regions, GMD values were calculated as the regions' volume (FIRST segmentations) divided by total intracranial volume. This resulted in a feature vector of 110 average GMD values (48 left cortical, 48 right cortical and 14 deep GM regions) and a feature vector of 20 average WMD values per subject.

DTI-based features were calculated by projecting each subject's FA, MD, AxD and RD values onto the TBSS group skeleton on a voxel-wise basis. Like the WMD features, the 20 WM tracts of the probabilistic JHU white-matter tractography atlas were then used to calculate a weighted mean value per tract per subject. This resulted in 4*20 feature vectors of mean FA, MD, AxD and RD values per subject.

In order to calculate the functional connectivity features, all processed rs-fMRI images were combined in a temporally concatenated independent component analysis (ICA (Beckmann and Smith, 2004)), with dimensionality fixed at 70 components and an ICA threshold of 0.99 (Smith et al., 2013). This meant that each voxel included in the ICA map was 99 times more likely to be part of that component than to be caused by Gaussian background noise. For each subject, we calculated the mean time course for each component, weighted by the ICA weight map and GM probability of that component's region. These mean time courses were subsequently used to determine the functional connectivity of a component with the 69 other components. Functional connectivity was either expressed as full correlations (FCor) or as sparse L1-regularised partial correlations (PCor) between the components' time courses. Partial correlations were calculated using the graphical lasso algorithm (Friedman et al., 2008). The functional connectivity measures resulted in two feature vectors of each (70*69)/2 = 2415 (partial) correlations per subject. Finally, we concatenated all feature vectors into one vector per subject.

2.6. BvFTD model

For our first analysis, a bvFTD patient-control classification model (Bouts et al., 2018) was applied to each subject's extracted feature vector. We applied the best performing, multimodal model that discriminated bvFTD patients from controls, which included the features GMD, FCor, FA, and MD (Bouts et al., 2018), as well as age and gender. Each subject's feature vector was fed into the model, resulting in a probability score from 0 to 1, where 0 represents a control subject and 1 represents a bvFTD patient. Extrapolated to our subjects, these scores showed how alike our presymptomatic FTD mutation carriers and healthy controls are to bvFTD patients.

Table 1
MRI sequence parameter settings.

	Slices	TR (ms)	TE (ms)	Flip angle (°)	Matrix (mm)	Voxel size (mm)	Duration (min)
3DT$_1$w	140	9.8	4.6	8	256 × 256	0.88 × 0.88 × 1.20	4.57
DWI[a]	70	8250	80	90	128 × 128	2.00 × 2.00 × 2.00	8.48
rs-fMRI	38	2200	30	80	80 × 80	2.75 × 2.75 × 2.99[b]	7.28

Scan protocol of whole-brain near-isotropic 3DT$_1$-weighted (3DT$_1$w), diffusion-weighted imaging (DWI), and resting-state functional MRI T$_{2*}$-weighted MRI (rs-fMRI) on a 3 T scanner at the Leiden University Medical Centre.
Abbreviations: TR: repetition time; TE: echo time.
[a] 60 directions, b = 1000, one b0 image.
[b] Including 10% interslice gap.

2.7. Carrier-control model

For the second analysis, feature vectors were used to train a logistic elastic net regression algorithm (Bouts et al., 2018; Zou and Hastie, 2005; Friedman et al., 2010; Schouten et al., 2016). The elastic net regression procedure estimates a sparse regression model that includes only a subset of the provided features by imposing a penalty for including features and for the weight of each feature. This way, elastic net provides a solution for the imbalance between the large number of features and the small number of subjects. Age and gender were included into the model without penalty to ensure that estimated feature regression coefficients were conditional on subject age and gender. Here, a probability score of 0 represented a control subject and 1 represented a presymptomatic FTD mutation carrier.

2.8. Cross-validation

Similarly to previous work (Bouts et al., 2018; Schouten et al., 2016), we trained our carrier-control model in a nested 10-fold cross-validation scheme to reduce classification bias. One part of the data (e.g. 10%) was set apart as a test set and served to test the generalised classification performance of the elastic net regression model. The remaining parts (90%) were used to train the model. However, in addition to the classification performance, we also wanted to determine the optimal penalty size without overestimating classification performance (Varma and Simon, 2006; Kriegeskorte et al., 2009). To this end, we used a second, nested 10-fold cross-validation loop on the training set over a grid of hyperparameters to determine the optimal penalty. In the nested loop, we estimated the model's hyperparameters that corresponded with the lowest binomial deviance, a goodness-of-fit measure that evaluates the difference between the predicted and actual observations. Next, these hyperparameters and corresponding penalties were used to train a model using the training set of the outer loop. Finally, the classification performance was tested on the test set of the outer loop. This process was repeated ten times to make sure that each subject was part of the test set at least once. Since the test set of the outer loop was neither used for model training, nor for parameter optimisation, potential prediction bias was reduced as much as possible (Kriegeskorte et al., 2009). The entire classification procedure was repeated 50 times to average classification outcome variability resulting from random partitioning in training and test folds. All classification analyses and evaluations were implemented in R version 3.3.2 (R core 2010, GLMnet package (Friedman et al., 2010)).

2.9. Classification performance

For both analyses, we quantified classification performances using receiver operating characteristic (ROC) curves. ROC curves were calculated by shifting the threshold for classifying an individual as patient (bvFTD model analysis) or carrier (carrier-control model analysis) from 0 to 1, and plotting the true positive rate (sensitivity) versus the false positivity (1 – specificity) for each intermediate point. The area under this ROC curve (AUC) is a measure of classification performance insensitive to the distribution between the groups (Fawcett, 2006). Additionally, we calculated the optimal operating point on the curve to calculate the model's sensitivity, specificity and classification accuracy, given equal class distribution and equal penalty for false positive and false negative predictions. For the carrier-control model analysis, we averaged AUC, accuracy, sensitivity and specificity values from the 50 times repeated nested cross-validations.

2.10. Multimodal classification

To obtain the best multimodal carrier-control model using several feature vectors, we performed step-wise feature concatenation as previously described (Bouts et al., 2018; Schouten et al., 2016). First, we

assessed classification performance for each feature separately. Subsequently, we added a new feature to the best performing feature combination (i.e. highest AUC) of the previous step until all features were included in the model. The best performing feature combination will be referred to as the multimodal carrier-control model.

2.11. Statistical analysis

Statistical analyses of non-imaging data were performed using R (R Core 2016, Vienna, Austria). We tested for carrier-control differences using unpaired t-tests (age and education), the Mann-Whitney U test (mini-mental state examination (MMSE) scores $[0-30]$) and the χ^2 test (gender distribution). Probability scores were compared using Mann-Whitney U tests for overall carrier-control contrasts, and Kruskal Wallis H tests and Dunn post-hoc tests for comparisons between all four groups (*MAPT*, *GRN*, *C9orf72* and controls). To compare models' AUC values against chance level, we used permutation tests ($N = 5.000$) (Noirhomme et al., 2014). In order to correct for multiple comparisons, we took the maximum AUC difference of the family of tests for each permutation. Then we compared the observed AUC difference to the new distribution of maximum AUC differences to get a family-wise error rate corrected p-value. The alpha level required for statistical significance was set at $p < 0.05$.

3. Results

3.1. Demographics

In total, 103 subjects met the inclusion criteria (Table 2). Mean age was similar for mutation carriers (52.0 ± 8.6 years) and healthy controls (54.2 ± 7.5 years). The proportion of female participants between mutation carriers (67%) and healthy controls (58%) was not different ($p = 0.3$). Education level was similar between groups (mutation carriers, 13.6 ± 2.9 years; healthy controls, 13.2 ± 2.4 years). MMSE was similarly distributed between groups (median [min-max], mutation carriers: 30 (Agosta et al., 2012; McMillan et al., 2012; McMillan et al., 2014; Mahoney et al., 2014; Daianu et al., 2016; Zhou et al., 2010; Zhou and Seeley, 2014), healthy controls: 29 (Agosta et al., 2012; McMillan et al., 2012; McMillan et al., 2014; Mahoney et al., 2014; Daianu et al., 2016; Zhou et al., 2010; Zhou and Seeley, 2014)).

3.2. BvFTD model

Application of the bvFTD model resulted in low bvFTD probability scores for most subjects (Fig. 1A), and the bvFTD probability scores were not significantly different in presymptomatic carriers (median = 0.038) than controls (median = 0.022, $p = 0.15$). ROC analysis of the bvFTD probabilities resulted in an AUC of 0.582, which was not significantly better than chance level ($p = 0.078$). Separated by gene (Fig. 1B), there were no differences between the four groups' bvFTD probability scores ($p = 0.37$). BvFTD probability scores of the original patients and controls used for cross-validation of the bvFTD

Table 2
Demographics.

	Carrier ($n = 55$)[a]	Control ($n = 48$)	P-value
Age[b]	52.0 (8.6)	54.2 (7.5)	0.2
Gender, ♀ (%)	37 (67%)	28 (58%)	0.3
Education, y[b,d]	13.6 (2.9)	13.2 (2.4)	0.5
MMSE[c]	30 (24–30)	29 (24–30)	0.5

Abbreviations: MMSE: mini-mental state examination.
[a] 8 MAPT, 35 GRN, 12 C9orf72.
[b] Values denote mean (standard deviation).
[c] Values denote median (range).
[d] Education values were missing for four carriers and two controls.

A. Classification by carrier status

B. Classification by genetic status
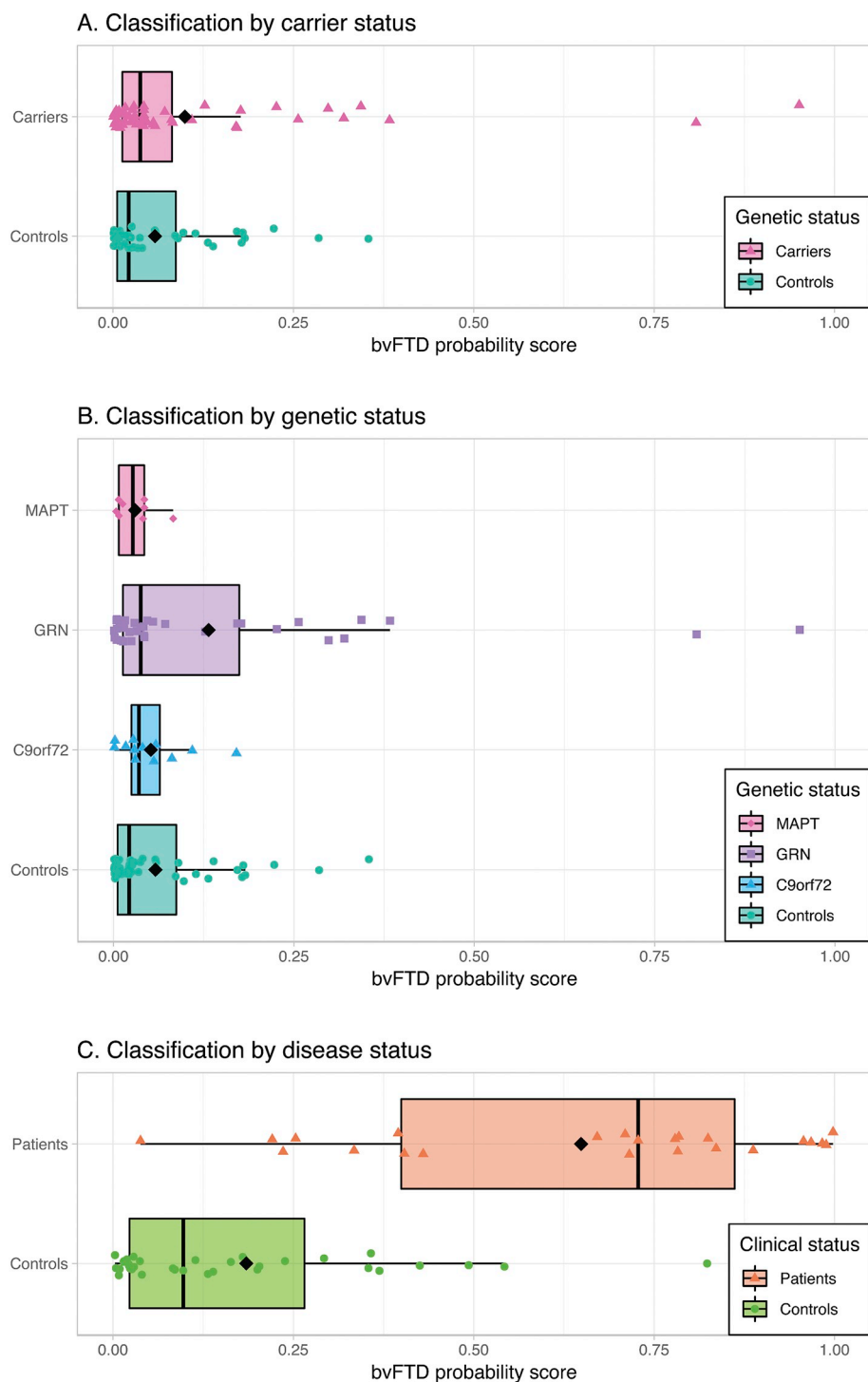

C. Classification by disease status

Fig. 1. Classification results bvFTD model.
Box and scatter plot of each subject's bvFTD probability score on a scale from 0 (representing control) to 1 (representing bvFTD patient) after application of the bvFTD model. Groups are defined by carrier status (Fig. 1A) and genetic status (Fig. 1B). Probability scores were not significantly different for carriers and controls ($p = 0.15$), and did not differ between the four genetic groups ($p = 0.37$). Probability score results of the bvFTD patients and controls on which the bvFTD model was cross-validated were added for reference (Fig. 1C, data courtesy of Bouts et al. (2018) (Bouts et al., 2018)). Abbreviations: *C9orf72*: chromosome 9 open reading frame 72; *GRN*: progranulin; *MAPT*: microtubule-associated protein tau.

model were added as reference (Fig. 1C, data courtesy of Bouts et al. (2018) (Bouts et al., 2018)).

3.3. Carrier-control model

The best performing unimodal carrier-control models included RD, WMD and MD, with AUCs of 0.642, 0.592, and 0.587, respectively. Of these models, only the RD model outperformed chance after family-wise error rate correction ($p = 0.032$, Table 3). Step-wise concatenation resulted in the best performing multimodal model, which included the features RD and WMD, and outperformed chance with an AUC of 0.684 ($p = 0.004$). Classification performance did not improve when

additional features were added to this model (Table 4). Interestingly, all multimodal models that outperformed chance level used exclusively white matter features from DTI and/or structural scans: RD, WMD, MD, and AxD).

Application of the best performing multimodal carrier-control model resulted in carrier probability scores (Fig. 2), which were different between carriers (median = 0.589) and controls (median = 0.435, $p < 0.001$, Fig. 2A). Furthermore, there was a difference between the four groups' carrier probability scores ($p = 0.008$) when separated by gene (Fig. 2B). Post-hoc tests revealed that *GRN* carriers had higher carrier probability scores than controls (Bonferroni family-wise error rate corrected $p = 0.009$). The other groups did not

Table 3
ROC characteristics.

Modality	AUC	Min – max	Sensitivity	Specificity	Accuracy	FWER Corr *P*-value (AUC > chance)
GMD	0.502	(0.427–0.554)	0.538	0.514	0.554	0.895
WMD	0.592	(0.547–0.656)	0.595	0.585	0.663	0.190
FA	0.494	(0.408–0.554)	0.528	0.504	0.535	0.897
MD	0.587	(0.523–0.629)	0.591	0.579	0.642	0.240
AxD	0.554	(0.500–0.598)	0.568	0.559	0.578	0.448
RD	*0.642*	(0.583–0.673)	0.637	0.629	0.669	*0.032*
FCor	0.509	(0.454–0.554)	0.537	0.527	0.590	0.818
PCor	0.505	(0.457–0.551)	0.542	0.492	0.540	0.836
Multimodal	***0.684***	(0.629–0.722)	0.664	0.640	0.735	***0.004***

Presymptomatic FTD mutation carriers versus controls classification. Multimodal represents the best combination from our step-wise multimodal procedure (i.e. RD & WMD). Bold: best-performing model. Italicised: mean AUC significantly higher than chance level after family-wise error rate correction.
Abbreviations: AxD: axial diffusivity; FA: fractional anisotropy; FCor: full correlations between ICA components; FWER Corr: family-wise error rate corrected; GMD: grey matter density; MD: mean diffusivity; PCor: L1-regularised partial correlations between ICA components; RD: radial diffusivity; WMD: white matter density; AUC: area under the ROC curve.

differ from each other.

4. Discussion

This study investigated whether presymptomatic FTD mutation carriers with *MAPT*, *GRN* and *C9orf72* mutations can be individually distinguished from healthy controls using MRI. Using a recently introduced MRI-based classification model trained on established bvFTD patients and controls, nearly all FTD mutation carriers and controls had low probability scores. The bvFTD model was therefore not able to separate carriers from controls beyond chance level. However, MRI-based classification models that were trained on our own sample were able to separate carriers from controls better than chance level. In our carrier-control model, the RD feature proved sufficient to separate carriers from controls better than chance, but the best performing model used RD in combination with the WMD feature. All models that outperformed chance used exclusively white matter features, such as DTI features and WMD, supporting the hypothesis that WM alterations are the first to appear in preclinical FTD pathology.

In an effort to improve on the FTD diagnostic criteria, single-subject classification using MRI measures has recently received significant attention (Möller et al., 2015b; McMillan et al., 2014; Davatzikos et al., 2008; Raamana et al., 2014; Koikkalainen et al., 2016; Wang et al., 2016; Meyer et al., 2017; Bron et al., 2017; Bouts et al., 2018). A recent multimodal classification study incorporated structural, DTI and arterial spin labelling data to classify FTD (behavioural and language variants) from cognitively normal controls, and achieved an AUC of 0.96 (Bron et al., 2017). Another classification study included tissue density, DTI and rs-fMRI measures, and achieved an AUC of 0.92 for bvFTD versus cognitively normal controls (Bouts et al., 2018). These

high classification performances are promising, but they are based on established FTD cases. It is unclear how FTD patient models generalise to earlier FTD stages, where brain alterations are less distinct. To test this, we applied a bvFTD model (Bouts et al., 2018) on FTD mutation carriers in a presymptomatic stage. We hypothesised that if the bvFTD model would be able to recognise early-stage FTD pathology, our presymptomatic FTD mutation carriers would have higher probability scores than controls. We found that it was not possible to separate carriers from controls significantly better than chance using this model, as most carriers and controls had very low bvFTD probability scores. This could indicate that presymptomatic differences present in FTD mutation carriers are too subtle to be picked up by a classification model that was trained established bvFTD patients. However, it could also mean that most of our mutation carriers were still too far from conversion to have significant FTD-related changes. Since the bvFTD model was trained on patients, it stands to reason that classification of carriers and controls becomes more accurate as mutation carriers approach conversion. Vice versa, one might expect the carriers with high probability scores to be closer to symptom-onset than carriers with lower probabilities. Although it was not statistically significant, there was a trend towards older age in carriers with a bvFTD probability score higher than 0.25 than in the rest of the carrier group (data not shown). It can therefore not be entirely ruled out that age is partly associated with a higher bvFTD score. Longitudinal research is warranted to formally test whether this model captures presymptomatic FTD-related changes as mutation carriers approach conversion.

By training classifiers on presymptomatic FTD mutation carriers and controls, we obtained a unimodal carrier-control model based on the RD feature and several multimodal carrier-control models that significantly outperformed chance level. This suggests that classification

Table 4
Multimodal classification performance.

Step: ddd combined with:	RD	WMD	MD	AxD	GMD	FA	FCor	PCor
1: –	*0.642*	0.592	0.587	0.554	0.502	0.494	0.509	0.505
2: RD	–	***0.684***	0.621	0.600	0.565	0.564	0.516	0.501
3: RD + WMD	–	–	*0.658*	*0.640*	0.596	0.607	0.520	0.501
4: RD + WMD + MD	–	–	–	0.627	0.612	0.614	0.524	0.502
5: RD + WMD + MD + AxD	–	–	–	–	0.612	0.609	0.531	0.507
6: RD + WMD + MD + AxD + GMD	–	–	–	–	–	0.585	0.534	0.509
7: RD + WMD + MD + AxD + GMD + FA	–	–	–	–	–	–	0.530	0.500
8: RD + WMD + MD + AxD + GMD + FA + FCor	–	–	–	–	–	–	–	0.510

Mean AUC values from 50 repetitions. Multimodal models result from step-wise addition of measures to the best performing classification model of the previous step, starting with the best performing single MRI measure (i.e. RD). Bold: best performing model. Italicised: mean AUC significantly higher than chance level after family-wise error rate correction.
Abbreviations: AxD: axial diffusivity; FA: fractional anisotropy; FCor: full correlations between ICA components; GMD: grey matter density; MD: mean diffusivity; PCor: L1-regularised partial correlations between ICA components; RD: radial diffusivity; WMD: white matter density; AUC: area under the ROC curve.

A. Classification by carrier status

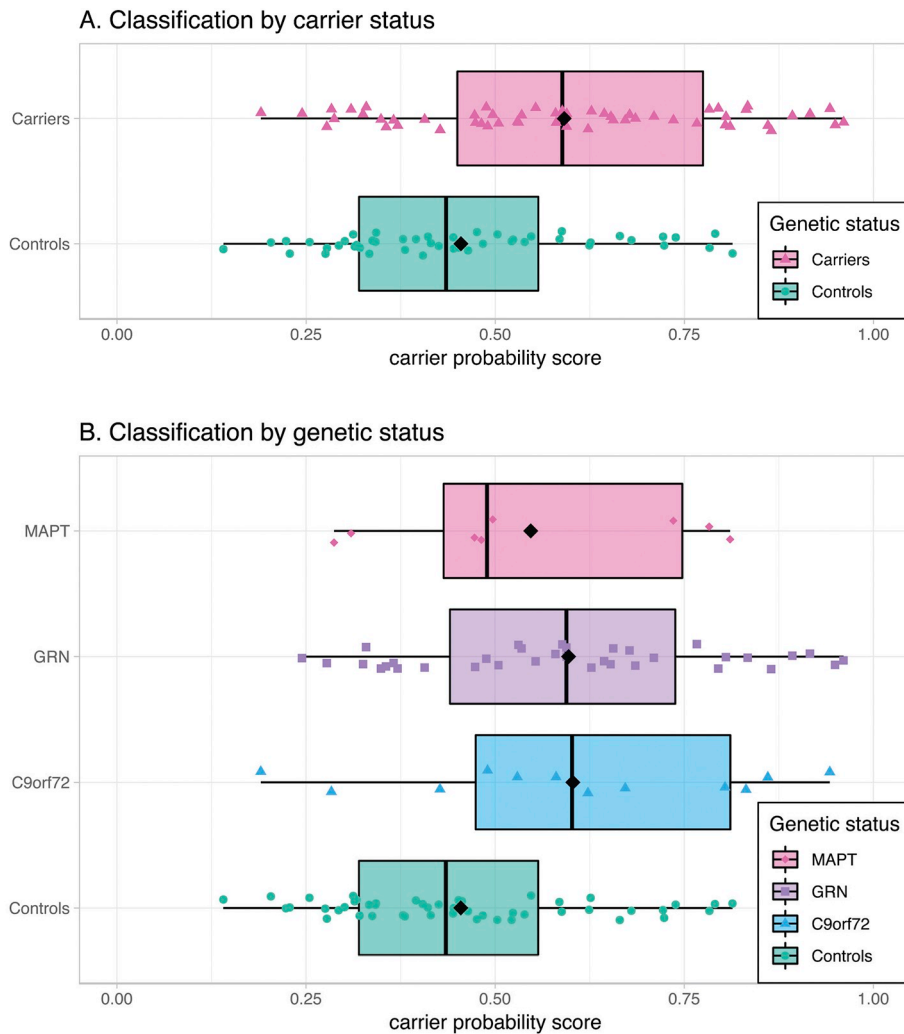## B. Classification by genetic status

Fig. 2. Classification results carrier-control model. Box and scatter plot of each subject's carrier probability score on a scale from 0 (representing control) to 1 (representing presymptomatic FTD mutation carrier) after application of the best performing carrier-control model including the features RD and WMD. Carriers had significantly higher scores than controls (Fig. 2A, $p < 0.001$). Furthermore, there was an omnibus difference between the four genetic groups (Fig. 2B, $p = 0.008$), and post-hoc tests revealed higher scores for *GRN* carriers than for controls ($p = 0.009$). Abbreviations: *C9orf72*: chromosome 9 open reading frame 72; *GRN*: progranulin; *MAPT*: microtubule-associated protein tau.

models should be trained using early-stage FTD patients or presymptomatic FTD mutation carriers instead of advanced FTD cases, in order to be sensitive to early-stage FTD pathology. Furthermore, our carrier-control models demonstrate that MRI-based machine learning is powerful enough to detect subtle pathological changes associated with FTD even before symptom-onset and on a single-subject level. Although classification performance beyond chance level is an important finding, it must be noted that AUCs of 0.642 and 0.684 are modest and far from sufficient for diagnostic use in the clinic. This is at least partly explained by our heterogeneous sample, as we included carriers of several genes in order to obtain sufficient sample size for robust cross-validation. Heterogeneity further arose from the uncertain time to onset in our sample. Investigating a uniform population a few years before symptom-onset might lead to higher classification performance, but these data were not available to us.

On a pathological level, it has been argued that neurodegeneration in FTD starts in the WM (Rohrer et al., 2013; Möller et al., 2016; Suri et al., 2014; Canu et al., 2017). Our results support this hypothesis, as the only unimodal model that outperformed chance was based on the RD feature, which was furthermore included in all multimodal models that significantly outperformed chance. Additionally, all models that outperformed chance level were based on DTI features, while three models also included WMD. This means that our carrier-control model was able to combine subtle WM differences from the diffusion-weighted scans and the structural 3DT1w scan to classify a subject as mutation carrier or healthy control. In our sample, inclusion of GMD and functional connectivity features did not aid classification, but in fact drove

down classification performance. For instance, adding FCor or PCor to the model resulted in probabilities near 0.5. This reinforces the notion that feature selection is important for MRI-based machine learning.

In addition to the uncertain time-to-onset, there were several other limitations. Firstly, the bvFTD model was trained on a relatively small sample of 23 bvFTD patients and 35 controls. A model based on a larger sample might capture the heterogeneity of bvFTD pathology more completely, which could benefit generalisation to our presymptomatic sample. Furthermore, the model was trained on sporadic bvFTD patients, while it was applied to carriers of *MAPT*, *GRN* and *C9orf72* genes. Since correlations between genetics, pathology and phenotype are not fully elucidated (Mann and Snowden, 2017), care must be taken not to over interpret our results. Specifically, pathological changes associated with non-behavioural variants (Seelaar et al., 2011) may be insufficiently recognised by the bvFTD model. Lastly, we used nested cross-validation to estimate out-of-sample performance for the carrier-control model, which minimises prediction bias (Kriegeskorte et al., 2009). Still, measuring performance on a separate validation cohort would further increase the validity of this study.

5. Conclusion

Our data show that presymptomatic FTD mutation carriers can be distinguished from healthy controls on an individual level using a new multimodal MRI-based carrier-control classification model, while this was not possible using a recent bvFTD classification model. A multimodal MRI-based classification score may therefore be a useful

biomarker to aid earlier FTD diagnosis. Successful single-subject recognition of early-stage or presymptomatic FTD may facilitate more precise subject recruitment into clinical trials. Furthermore, our multimodal MRI-based carrier-control classification model supports the hypothesis that FTD-related neurodegeneration starts in WM.

Acknowledgements

References

Agosta, F., Scola, E., Canu, E., Marcone, A., Magnani, G., Sarro, L., et al., 2012. White matter damage in frontotemporal lobar degeneration spectrum. Cereb. Cortex 22 (12), 2705–2714.

Anderson, J.L.R., Jenkinson, M., Smith, S., 2007. Non-Linear Registration Aka Spatial Normalisation. FMRIB Centre, Oxford, United Kingdom (FMRIB Technical Report TR07JA2.).

Beckmann, C.F., Smith, S.M., 2004 Feb. Probabilistic independent component analysis for functional magnetic resonance imaging. IEEE Trans. Med. Imaging 23 (2), 137–152.

Bertrand, A., Wen, J., Rinaldi, D., Houot, M., Sayah, S., Camuzat, A., et al., 2018 Feb 1. Early cognitive, structural, and microstructural changes in Presymptomatic C9orf72 carriers younger than 40 years. JAMA Neurol. 75 (2), 236–245.

Borroni, B., Alberici, A., Premi, E., Archetti, S., Garibotto, V., Agosti, C., et al., 2008 Jun. Brain magnetic resonance imaging structural changes in a pedigree of asymptomatic progranulin mutation carriers. Rejuvenation Res. 11 (3), 585–595.

Borroni, B., Alberici, A., Cercignani, M., Premi, E., Serra, L., Cerini, C., et al., 2012. Granulin mutation drives brain damage and reorganization from preclinical to symptomatic FTLD. Neurobiol. Aging 33 (10), 2506–2520.

Bouts, M.J.R.J., Möller, C., Hafkemeijer, A., van Swieten, J.C., Dopper, E., van der Flier, W.M., et al., 2018 Mar 27. Single subject classification of Alzheimer's disease and Behavioral variant Frontotemporal dementia using anatomical, diffusion tensor, and resting-state functional magnetic resonance imaging. J. Alzheimers Dis. 62 (4), 1827–1839 (Zhang Y, editor.).

Bron, E.E., Smits, M., Papma, J.M., Steketee, R.M.E., Meijboom, R., de Groot, M., et al., 2017 Aug 16. Multiparametric computer-aided differential diagnosis of Alzheimer's disease and frontotemporal dementia using structural and advanced MRI. Eur. Radiol. 27 (8), 3372–3382.

Canu, E., Agosta, F., Mandic-Stojmenovic, G., Stojković, T., Stefanova, E., Inuggi, A., et al., 2017. Multiparametric MRI to distinguish early onset Alzheimer's disease and behavioral variant of frontotemporal dementia. Neuroimaging Clin. 15, 428–438.

Cash, D.M., Bocchetta, M., Thomas, D.L., Dick, K.M., van Swieten, J.C., Borroni, B., et al., 2018 Feb 1. Patterns of gray matter atrophy in genetic frontotemporal dementia: results from the GENFI study. Neurobiol. Aging 62, 191–196.

Chao, L.L., Schuff, N., Clevenger, E.M., Mueller, S.G., Rosen, H.J., Gorno-Tempini, M.L., et al., 2007 Nov 1. Patterns of white matter atrophy in Frontotemporal lobar degeneration. Arch. Neurol. 64 (11), 1619.

Daianu, M., Mendez, M.F., Baboyan, V.G., Jin, Y., Melrose, R.J., Jimenez, E.E., et al., 2016 Oct 29. An advanced white matter tract analysis in frontotemporal dementia and early-onset Alzheimer's disease. Brain Imaging Behav. 10 (4), 1038–1053.

Davatzikos, C., Resnick, S.M., Wu, X., Parmpi, P., Clark, C.M., 2008 Jul. Individual patient diagnosis of AD and FTD via high-dimensional pattern classification of MRI. NeuroImage 41 (4), 1220–1227.

Dopper, E.G.P., Rombouts, S.A.R.B., Jiskoot, L.C., den Heijer, T., de Graaf, J.R.A., de Koning, I., et al., 2014 Jul 8. Structural and functional brain connectivity in presymptomatic familial frontotemporal dementia. Neurology 83 (2), e19–e26.

Farb, N.A.S., Grady, C.L., Strother, S., Tang-Wai, D.F., Masellis, M., Black, S., et al., 2013 Jul. Abnormal network connectivity in frontotemporal dementia: evidence for prefrontal isolation. Cortex 49 (7), 1856–1873.

Fawcett, T., 2006 Jun 1. An introduction to ROC analysis. Pattern Recogn. Lett. 27 (8), 861–874.

Friedman, J., Hastie, T., Tibshirani, R., 2008 Jul. Sparse inverse covariance estimation with the graphical lasso. Biostatistics 9 (3), 432–441.

Friedman, J., Hastie, T., Tibshirani, R., 2010. Regularization paths for generalized linear models via coordinate descent. J. Stat. Softw. 33 (1), 1–22.

Frings, L., Yew, B., Flanagan, E., Lam, B.Y.K., Hüll, M., Huppertz, H.-J., et al., 2014 Mar 3. Longitudinal grey and white matter changes in frontotemporal dementia and Alzheimer's disease. PLoS One 9 (3), e90814 (Esteban FJ, editor.).

Friston, K.J., Ashburner, J., Kiebel, S., Nichols, T., Penny, W.D., 2007. Statistical Parametric Mapping : the Analysis of Funtional Brain Images. Elsevier/Academic Press, pp. 647.

Gorno-Tempini, M.L.L., Hillis a, E.E., Weintraub, S., Kertesz, A., Mendez, M., Cappa, S.F.F., et al., 2011. Classification of primary progressive aphasia and its variants. Neurology 76 (11), 1006–1014.

Greve, D.N., Fischl, B., 2009 Oct. Accurate and robust brain image alignment using boundary-based registration. NeuroImage 48 (1), 63–72.

Hafkemeijer, A., Möller, C., Dopper, E.G.P., Jiskoot, L.C., Schouten, T.M., van Swieten, J.C., et al., 2015. Resting state functional connectivity differences between behavioral variant frontotemporal dementia and Alzheimer's disease. Front. Hum. Neurosci. 9, 474.

Hafkemeijer, A., Möller, C., Dopper, E.G.P., Jiskoot, L.C., van den Berg-Huysmans, A.A., van Swieten, J.C., et al., 2016. Differences in structural covariance brain networks between behavioral variant frontotemporal dementia and Alzheimer's disease. Hum. Brain Mapp. 37 (3), 978–988.

Harvey, R.J., Skelton-Robinson, M., Rossor, M.N., 2003 Sep. The prevalence and causes of dementia in people under the age of 65 years. J. Neurol. Neurosurg. Psychiatry 74 (9), 1206–1209.

Huey, E.D., Armstrong, N., Momeni, P., Grafman, J., 2008 Nov 14. Challenges and new opportunities in the investigation of new drug therapies to treat frontotemporal dementia. Expert Opin. Ther. Targets 12 (11), 1367–1376.

Jenkinson, M., Bannister, P., Brady, M., Smith, S., 2002. Improved optimization for the robust and accurate linear registration and motion correction of brain images. NeuroImage 17 (2), 825–841.

Jiskoot, L.C., Dopper, E.G.P., den Heijer, T., Timman, R., van Minkelen, R., van Swieten, J.C., et al., 2016 Jul 26. Presymptomatic cognitive decline in familial frontotemporal dementia: a longitudinal study. Neurology 87 (4), 384–391.

Koikkalainen, J., Rhodius-Meester, H., Tolonen, A., Barkhof, F., Tijms, B., Lemstra, A.W., et al., 2016. Differential diagnosis of neurodegenerative diseases using structural MRI data. Neuroimaging Clin. 11, 435–449.

Kriegeskorte, N., Simmons, W.K., Bellgowan, P.S.F., Baker, C.I., 2009 May. Circular analysis in systems neuroscience: the dangers of double dipping. Nat. Neurosci. 12 (5), 535–540.

Lee, S.E., Khazenzon, A.M., Trujillo, A.J., Guo, C.C., Yokoyama, J.S., Sha, S.J., et al., 2014 Nov. Altered network connectivity in frontotemporal dementia with C9orf72 hexanucleotide repeat expansion. Brain 137 (11), 3047–3060.

Lee, S.E., Sias, A.C., Mandelli, M.L., Brown, J.A., Brown, A.B., Khazenzon, A.M., et al., 2017. Network degeneration and dysfunction in presymptomatic C9ORF72 expansion carriers. Neuroimaging Clin. 14, 286–297.

Leemans, A., Jones, D.K., 2009 Jun 1. The B-matrix must be rotated when correcting for subject motion in DTI data. Magn. Reson. Med. 61 (6), 1336–1349.

Ludolph, A., Drory, V., Hardiman, O., Nakano, I., Ravits, J., Robberecht, W., et al., 2015 Aug 27. A revision of the El Escorial criteria - 2015. Amyotroph. Lateral Scler. Front Degener. 16 (5–6), 291–292.

Mahoney, C.J., Ridgway, G.R., Malone, I.B., Downey, L.E., Beck, J., Kinnunen, K.M., et al., 2014. Profiles of white matter tract pathology in frontotemporal dementia. Hum. Brain Mapp. 35 (8), 4163–4179.

Mann, D.M.A., Snowden, J.S., 2017 Nov 1. Frontotemporal lobar degeneration: pathogenesis, pathology and pathways to phenotype. Brain Pathol. 27 (6), 723–736.

McMillan, C.T., Brun, C., Siddiqui, S., Churgin, M., Libon, D., Yushkevich, P., et al., 2012 May 29. White matter imaging contributes to the multimodal diagnosis of frontotemporal lobar degeneration. Neurology 78 (22), 1761–1768.

McMillan, C.T., Avants, B.B., Cook, P., Ungar, L., Trojanowski, J.Q., Grossman, M., 2014 Sep 1. The power of neuroimaging biomarkers for screening frontotemporal dementia. Hum. Brain Mapp. 35 (9), 4827–4840.

Mendez, M.F., 2009. Frontotemporal dementia: therapeutic interventions. In: Dementia in Clinical Practice. KARGER, Basel, pp. 168–178.

Mendez, M.F., Shapira, J.S., McMurtray, A., Licht, E., Miller, B.L., BL, M., et al., 2007 Jun 1. Accuracy of the clinical evaluation for frontotemporal dementia. Arch. Neurol. 64 (6), 830.

Meyer, S., Mueller, K., Stuke, K., Bisenius, S., Diehl-Schmid, J., Jessen, F., et al., 2017. Predicting behavioral variant frontotemporal dementia with pattern classification in multi-center structural MRI data. Neuroimaging Clin. 14, 656–662.

Mohs, R.C., Doody, R.S., Morris, J.C., Ieni, J.R., Rogers, S.L., Perdomo, C.A., et al., 2001 Aug 14. A 1-year, placebo-controlled preservation of function survival study of donepezil in AD patients. Neurology 57 (3), 481–488.

Möller, C., Dieleman, N., Van Der Flier, W.M., Versteeg, A., Pijnenburg, Y., Scheltens, P., et al., 2015a. More atrophy of deep Gray matter structures in Frontotemporal dementia compared to Alzheimer's disease. J. Alzheimers Dis. 44 (2), 635–647.

Möller, C., Hafkemeijer, A., Pijnenburg, Y.A.L., Rombouts, S.A.R.B., Van Der Grond, J., Dopper, E., et al., 2015b. Joint assessment of white matter integrity, cortical and subcortical atrophy to distinguish AD from behavioral variant FTD: a two-center study. Neuroimaging Clin. 9, 418–429.

Möller, C., Pijnenburg, Y.A.L., van der Flier, W.M., Versteeg, A., Tijms, B., de Munck, J.C., et al., 2016 Jun. Alzheimer disease and Behavioral variant Frontotemporal dementia: automatic classification based on cortical atrophy for single-subject diagnosis. Radiology 279 (3), 838–848.

Noirhomme, Q., Lesenfants, D., Gomez, F., Soddu, A., Schrouff, J., Garraux, G., et al., 2014. Biased binomial assessment of cross-validated estimation of classification accuracies illustrated in diagnosis predictions. Neuroimaging Clin. 4, 687–694.

Pan, P.L., Song, W., Yang, J., Huang, R., Chen, K., Gong, Q.Y., et al., 2012. Gray matter atrophy in behavioral variant frontotemporal dementia: a meta-analysis of voxel-based morphometry studies. Dement. Geriatr. Cogn. Disord. 33 (2–3), 141–148.

Papma, J.M., Jiskoot, L.C., Panman, J.L., Dopper, E.G., den Heijer, T., Donker Kaat, L., et al., 2017 Sep 19. Cognition and gray and white matter characteristics of presymptomatic C9orf72 repeat expansion. Neurology 89 (12), 1256–1264.

Patenaude, B., Smith, S.M., Kennedy, D.N., Jenkinson, M., 2011 Jun. A Bayesian model of shape and appearance for subcortical brain segmentation. NeuroImage 56 (3), 907–922.

Premi, E., Cauda, F., Gasparotti, R., Diano, M., Archetti, S., Padovani, A., et al., 2014 Sep 4. Multimodal fMRI resting-state functional connectivity in granulin mutations: the case of fronto-parietal dementia. PLoS One 9 (9), e106500 (Zang Y-F, editor.).

Pressman, P.S., Miller, B.L., 2014 Apr. Diagnosis and management of behavioral variant frontotemporal dementia. Biol. Psychiatry 75 (7), 574–581.

Pruim, R.H.R., Mennes, M., van Rooij, D., Llera, A., Buitelaar, J.K., Beckmann, C.F., 2015 May 15. ICA-AROMA: a robust ICA-based strategy for removing motion artifacts from fMRI data. NeuroImage 112, 267–277.

Raamana, P.R., Rosen, H., Miller, B., Weiner, M.W., Wang, L., Beg, M.F., 2014 May 12. Three-class differential diagnosis among Alzheimer disease, Frontotemporal dementia, and controls. Front. Neurol. 5, 71.

Rabinovici, G.D., Miller, B.L., 2010 May. Frontotemporal lobar degeneration. CNS Drugs. 24 (5), 375–398.

Rabinovici, G.D., Seeley, W.W., Kim, E.J., Gorno-Tempini, M.L., Rascovsky, K., Pagliaro, T.A., et al., 2008 Dec 1. Distinct MRI atrophy patterns in autopsy-proven Alzheimer's disease and frontotemporal lobar degeneration. Am. J. Alzheimer Dis. Other Dementiasr 22 (6), 474–488.

Rascovsky, K., Hodges, J.R., Knopman, D., Mendez, M.F., Kramer, J.H., Neuhaus, J., et al., 2011 Sep. Sensitivity of revised diagnostic criteria for the behavioural variant of frontotemporal dementia. Brain 134 (Pt 9), 2456–2477.

Ratnavalli, E., Brayne, C., Dawson, K., Hodges, J.R., 2002 Jun. The prevalence of frontotemporal dementia. Neurology 58 (11), 1615–1621.

Risacher, S., Saykin, A., 2013 Nov 14. Neuroimaging biomarkers of neurodegenerative diseases and dementia. Semin. Neurol. 33 (04), 386–416.

Rohrer, J.D., Warren, J.D., Fox, N.C., Rossor, M.N., 2013 Oct. Presymptomatic studies in genetic frontotemporal dementia. Rev. Neurol. 169 (10), 820–824.

Rohrer, J.D., Nicholas, J.M., Cash, D.M., van Swieten, J., Dopper, E., Jiskoot, L., et al., 2015. Presymptomatic cognitive and neuroanatomical changes in genetic frontotemporal dementia in the genetic Frontotemporal dementia initiative (GENFI) study: a cross-sectional analysis. Lancet Neurol. 14 (3), 253–262.

Schouten, T.M., Koini, M., de Vos, F., Seiler, S., van der Grond, J., Lechner, A., et al., 2016. Combining anatomical, diffusion, and resting state functional magnetic resonance imaging for individual classification of mild and moderate Alzheimer's disease. Neuroimaging Clin. 11, 46–51.

Seelaar, H., Rohrer, J.D., Pijnenburg, Y.A.L., Fox, N.C., Van Swieten, J.C., 2011 May 1. Clinical, genetic and pathological heterogeneity of frontotemporal dementia: a review. J. Neurol. Neurosurg. Psychiatry 82 (5), 476–486.

Seeley, W.W., Crawford, R.K., Zhou, J., Miller, B.L., Greicius, M.D., 2009 Apr. Neurodegenerative diseases target large-scale human brain networks. Neuron 62 (1), 42–52.

Smith, S.M., 2002 Nov. Fast robust automated brain extraction. Hum. Brain Mapp. 17 (3), 143–155.

Smith, S.M., Jenkinson, M., Woolrich, M.W., Beckmann, C.F., Behrens, T.E.J., Johansen-Berg, H., et al., 2004. Advances in functional and structural MR image analysis and implementation as FSL. NeuroImage 23 (Suppl. 1), 208–219.

Smith, S.M., Jenkinson, M., Johansen-Berg, H., Rueckert, D., Nichols, T.E., Mackay, C.E., et al., 2006 Jul. Tract-based spatial statistics: voxelwise analysis of multi-subject diffusion data. NeuroImage 31 (4), 1487–1505.

Smith, S.M., Beckmann, C.F., Andersson, J., Auerbach, E.J., Bijsterbosch, J., Douaud, G., et al., 2013. Resting-state fMRI in the human Connectome project. NeuroImage 80, 144–168.

Suri, S., Topiwala, A., Mackay, C.E., Ebmeier, K.P., Filippini, N., 2014 Sep 17. Using structural and diffusion magnetic resonance imaging to differentiate the dementias. Curr. Neurol. Neurosci. Rep. 14 (9), 475.

Tustison, N.J., Avants, B.B., Cook, P.A., Zheng, Yuanjie, Egan, A., Yushkevich, P.A., et al., 2010 Jun. N4ITK: improved N3 Bias correction. IEEE Trans. Med. Imaging 29 (6), 1310–1320.

Varma, S., Simon, R., 2006 Feb 23. Bias in error estimation when using cross-validation for model selection. BMC Bioinformatics. 7, 91.

Wang, J., Redmond, S.J., Bertoux, M., Hodges, J.R., Hornberger, M., 2016 Jun 16. A comparison of magnetic resonance imaging and neuropsychological examination in the diagnostic distinction of Alzheimer's disease and Behavioral variant Frontotemporal dementia. Front. Aging Neurosci. 8, 119.

Whitwell, J.L., Jack, C.R., 2005. Comparisons between Alzheimer disease, frontotemporal lobar degeneration, and normal aging with brain mapping. Top. Magn. Reson. Imaging 16 (6), 409–425.

Whitwell, J.L., Josephs, K.A., Avula, R., Tosakulwong, N., Weigand, S.D., Senjem, M.L., et al., 2011 Aug. Altered functional connectivity in asymptomatic MAPT subjects: a comparison to bvFTD. Neurology 77 (9), 866–874.

Whitwell, J.L., Weigand, S.D., Boeve, B.F., Senjem, M.L., Gunter, J.L., DeJesus-Hernandez, M., et al., 2012 Mar 1. Neuroimaging signatures of frontotemporal dementia genetics: C9ORF72, tau, progranulin and sporadics. Brain 135 (3), 794–806.

Whitwell, J.L., Boeve, B.F., Weigand, S.D., Senjem, M.L., Gunter, J.L., Baker, M.C., et al., 2015. Brain atrophy over time in genetic and sporadic frontotemporal dementia: a study of 198 serial magnetic resonance images. Eur. J. Neurol. 22 (5), 745–752.

Zhang, Y., Schuff, N., Du, A.-T., Rosen, H.J., Kramer, J.H., Gorno-Tempini, M.L., et al., 2009. White matter damage in frontotemporal dementia and Alzheimer's disease measured by diffusion MRI. Brain 132 (Pt 9), 2579–2592.

Zhang, Y., Schuff, N., Ching, C., Tosun, D., Zhan, W., Nezamzadeh, M., et al., 2011 Jun 27. Joint assessment of structural, perfusion, and diffusion MRI in Alzheimer's disease and frontotemporal dementia. Int. J. Alzheimers Dis. 2011, 11.

Zhou, J., Seeley, W.W., 2014 Apr. Network dysfunction in Alzheimer's disease and Frontotemporal dementia: implications for psychiatry. Biol. Psychiatry 75 (7), 565–573.

Zhou, J., Greicius, M.D., Gennatas, E.D., Growdon, M.E., Jang, J.Y., Rabinovici, G.D., et al., 2010 May. Divergent network connectivity changes in behavioural variant frontotemporal dementia and Alzheimer's disease. Brain 133 (Pt 5), 1352–1367.

Zou, H., Hastie, T., 2005 Apr 1. Regularization and variable selection via the elastic net. J. R. Stat. Soc. Ser. B 67 (2), 301–320 (Statistical Methodol.).